

Fundamental Limits of Thermal-noise Lossy Bosonic Multiple Access Channel

Evan J.D. Anderson
Optical Sciences

University of Arizona
Tucson Arizona, USA
ejdanderson@optics.arizona.edu

Boulat A. Bash

Electrical & Computer Engineering, Optical Sciences
University of Arizona
Tucson Arizona, USA
boulat@arizona.edu

Abstract—We develop the capacity region for the bosonic multiple access channel (MAC) in the presence of thermal-noise added by the environment. Bosonic channel describes quantum-mechanically many practical communication links such as optical, microwave, and radiofrequency. We find that, the use of single-mode squeezed states can increase the capacity over that afforded by coherent state encoding when each transmitter is photon-number constrained individually. However, the benefit disappears in the asymptotic regimes of high and low signal-to-noise ratio. Additionally, under a combined total photon-number constraint at the transmitters, no benefit from squeezing is observed over the use of coherent states.

I. INTRODUCTION

The multiple access channel (MAC) is the principal building block of many practical networks. Quantum information [1], [2] governs the fundamental limits of physical channels comprising any network, and offers substantial benefits in their performance [3]–[6] and security [7]–[11]. While the MAC has been studied extensively in classical network information theory [12], the quantum perspective has been underexplored. With notable exception of [13], [14], previous work has largely focused on the quantum channels that act on finite-dimensional qudits [15]–[17]. While recent results focused on coding [18]–[20], entanglement-assisted communication [21]–[24], and secrecy [25], [26], there is a gap in understanding of the fundamental limits of the bosonic multiple access communication in the presence of thermal-noise.

Previous work characterized the classical capacity region for the pure loss bosonic MAC when no excess noise was injected by the environment [13], [14]. However, such a model does not completely describe practical communication systems. Here, we derive the capacity region for classical communication over the bosonic MAC, accounting for both the thermal-noise added by the environment and signal lost to it. We explore the impact of using single-mode squeezed states on the MAC capacity. While bosonic channels model quantum-mechanically many practical channels (including free-space and fiber optical, microwave, and radiofrequency (RF)), they are particularly useful in optical communications. This is because noises of quantum-mechanical origin limit the performance of advanced high-sensitivity photodetection systems [27]–[29] and the bosonic

MAC in particular accurately represents high-speed optical interconnects between and within silicon microchips. Furthermore, quantum methodology includes resources such as squeezed states, shared entanglement, and joint detection receivers that can substantially increase communication capacity. Indeed, the bosonic channel model allows the fundamental limits in throughput and security to be explored by lifting all the assumptions on the transceiver and the adversary except those allowed by the laws of physics.

After formally defining our channel model and stating necessary previous technical results in Section II, we build on [13], [14] to develop the lossy thermal-noise bosonic MAC capacity region in Section III. We focus on exploring the use of single-mode squeezed states and find that, although their use can increase the capacity under individual photon-number constraints on communicating parties when the channel parameters are fixed, their benefit disappears in the asymptotic regimes of high and low signal-to-noise ratio (SNR). We also show that under a combined photon-number constraint, no benefit is achieved using squeezed states over coherent states. We conclude in Section IV with discussion of the implications of our results of future work.

II. PRELIMINARIES

A. Channel Model

Consider a channel depicted in Fig. 1(a). The transmissivity η of the beamsplitter models the power coupling between transmitter Alice (\hat{a}) and receiver Charlie (\hat{c}). Alice and the environment (\hat{b}) inject signal and noise states into their respective input ports described by modal annihilation operators \hat{a} and \hat{b} (as is customary in the literature, we ignore the system's phase shift $e^{i\phi}$, setting $\phi = 0$). Charlie's output modal annihilation operator is given by $\hat{c} = \sqrt{\eta}\hat{a} + \sqrt{1-\eta}\hat{b}$. When the environment is in a vacuum state $|0\rangle\langle 0|$, Fig. 1(a) depicts a *pure-loss*, or lossy bosonic channel, when it is in a thermal state (formally described in Sec. II-A), Fig. 1(a) depicts a *lossy thermal-noise* bosonic channel. Such point-to-point bosonic channels are well-studied [3]–[6], [30], [31], [32, Sec. V].

When a second transmitter, Bob, replaces the environment, the setup in Fig. 1(a) represents lossy bosonic MAC. This channel was analyzed by Yen and Shapiro in [13], [14], and

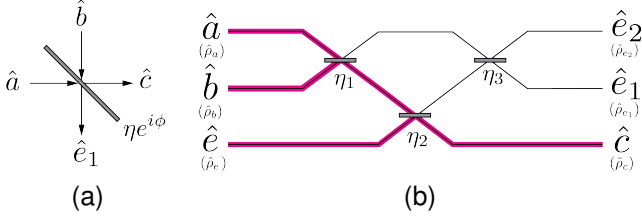


Fig. 1. a) Single-mode bosonic channel modeled by a beamsplitter with transmissivity η , phase shift $e^{i\phi}$, and modal input and output annihilation operators \hat{a} , \hat{b} , \hat{c} , and \hat{e}_1 . We assume a known phase set to $\phi = 0$. b) The generalized three-input, three-output lossy thermal-noise channel model. Input modal annihilation operators \hat{a} and \hat{b} represent transmitters Alice and Bob while the third \hat{e} is the environment. The receiver, Charlie, is modeled by modal annihilation operator \hat{c} while \hat{e}_1, \hat{e}_2 represent photon loss to the environment. The path photons take from each of the input modes through the beamsplitters and arrive at the receiver is highlighted.

our work builds on their results summarized in Section II-D. However, the applications of the lossy bosonic MAC in [13], [14] are limited to systems that are not afflicted by excess thermal-noise. Including thermal noise results in a richer model. Therefore, in this paper, we include thermal noise by generalizing the two-input two-output bosonic channel model in Fig. 1(a) to K inputs and outputs. The general thermal-noise lossy bosonic MAC is modeled by K input modes ($K - 1$ transmitters, 1 environment mode) and K output modes (1 receiver and $K - 1$ environment modes that are traced out accounting for photon loss to the environment). We require a minimum of $\frac{K(K-1)}{2}$ arbitrary beamsplitters with transmissivity η_i , $i = 1, 2, \dots, \frac{K(K-1)}{2}$ [33]. Here, for simplicity of exposition, we set $K = 3$ as seen in Fig. 1(b), noting that our analysis is generalizable to $K > 3$. The modal relationship between the input modes and the output mode at the receiver is given by:

$$\hat{c} = \sqrt{\eta_1 \eta_2} \hat{a} + \sqrt{(1 - \eta_1) \eta_2} \hat{b} + \sqrt{1 - \eta_2} \hat{e}. \quad (1)$$

B. Gaussian Quantum Information

We consider Gaussian-state inputs and outputs. A single-mode quantum state $\hat{\rho}$ is called Gaussian if its Wigner function is of the form [32]

$$W(\boldsymbol{\mu}) = \frac{\exp\left[-\frac{1}{2}(\boldsymbol{\mu} - \bar{\boldsymbol{\mu}})^\top \boldsymbol{\Sigma}^{-1}(\boldsymbol{\mu} - \bar{\boldsymbol{\mu}})\right]}{2\pi \sqrt{|\boldsymbol{\Sigma}|}} \quad (2)$$

where $|\mathbf{A}|$ and \mathbf{A}^\top respectively denote the determinant and transpose of matrix \mathbf{A} . The mean (displacement) $\bar{\boldsymbol{\mu}} = [\bar{\mu}_1 \ \bar{\mu}_2]^\top$ and covariance matrix $\boldsymbol{\Sigma} = \begin{bmatrix} \sigma_{11}^2 & \sigma_{12}^2 \\ \sigma_{21}^2 & \sigma_{22}^2 \end{bmatrix}$ are calculated with respect to quadrature components $\hat{p} = \text{Im}(\hat{a})$ and $\hat{q} = \text{Re}(\hat{a})$ of the annihilation operator \hat{a} . Then, $\bar{\boldsymbol{\mu}}$ and $\boldsymbol{\Sigma}$ fully characterize $\hat{\rho}$. We do not employ entanglement between quadratures, setting $\sigma_{12}^2 = \sigma_{21}^2 = 0$. States of particular interest to us are:

- vacuum states: $\bar{\boldsymbol{\mu}} = 0, \sigma_{11}^2 = \sigma_{22}^2 = \frac{1}{4}$
- coherent states: $|\bar{\boldsymbol{\mu}}\rangle > 0, \sigma_{11}^2 = \sigma_{22}^2 = \frac{1}{4}$
- single-mode squeezed states: $|\bar{\boldsymbol{\mu}}\rangle \geq 0, \sigma_{11}^2 = \frac{1}{4}e^{2r}, \sigma_{22}^2 = \frac{1}{4}e^{-2r}$ where $r \in \mathbb{R}$ is the squeezing parameter

- thermal states: $\bar{\boldsymbol{\mu}} = 0, \sigma_{11}^2 = \sigma_{22}^2 = \frac{1}{2}(\bar{n}_T + \frac{1}{2})$ where $\bar{n}_T > 0$ is the mean photon number.

The squeezed, coherent, and vacuum states are minimum uncertainty states, the product of their quadrature variances is $\frac{1}{16}$. When squeezing in one quadrature the uncertainty in that quadrature is decreased while the other is increased at the cost of $\frac{1}{4}(e^{2r} + e^{-2r}) - \frac{1}{2} = \frac{1}{2} \cosh(2r) - \frac{1}{2}$ additional photons.

The generalized bosonic channel described in Section II-A preserves Gaussianity which is shown via characteristic functions. Thus, if Alice and Bob employ Gaussian input states, then Charlie's state is also Gaussian. Alice and Bob encode their signal by performing a displacement on a zero-mean Gaussian state. This displacement utilizes \bar{n}_α and \bar{n}_β mean photon numbers from Alice and Bob respectively. The observed mean photon number of the signal at the receiver is given by

$$\bar{n}_C = \eta_1 \eta_2 \bar{n}_\alpha + (1 - \eta_1) \eta_2 \bar{n}_\beta. \quad (3)$$

The covariance matrix at the receiver in terms of the covariance matrices of the three inputs is similarly given by:

$$\mathbf{V} = \eta_1 \eta_2 \mathbf{X} + (1 - \eta_1) \eta_2 \mathbf{Y} + (1 - \eta_2) \mathbf{Z}, \quad (4)$$

where

$$\mathbf{X} = \frac{1}{4} \begin{bmatrix} e^{2r_A} & 0 \\ 0 & e^{-2r_A} \end{bmatrix}, \quad \mathbf{Y} = \frac{1}{4} \begin{bmatrix} e^{2r_B} & 0 \\ 0 & e^{-2r_B} \end{bmatrix} \quad (5)$$

$$\mathbf{Z} = \frac{1}{4} \begin{bmatrix} 2\bar{n}_T + 1 & 0 \\ 0 & 2\bar{n}_T + 1 \end{bmatrix}, \quad \mathbf{V} = \begin{bmatrix} V_{11} & V_{12} \\ V_{12} & V_{22} \end{bmatrix}.$$

Alice and Bob's squeezing parameters are given by r_A, r_B respectively, $\mathbf{X}, \mathbf{Y}, \mathbf{Z}$ are the covariance matrices for the input modes of the two transmitters and environment respectively, and \mathbf{V} is the covariance matrix at Charlie's output mode \hat{c} .

Additionally, if Alice is constrained to mean photon number \bar{n}_A , then she can only use $\bar{n}_\alpha = \bar{n}_A - \frac{1}{2} \cosh(2r_A) + \frac{1}{2} = \bar{n}_A - X_1 - X_2 + \frac{1}{2}$ photons for modulating the mean of their Gaussian input state with the rest of the photons reserved for squeezing when $r_A \neq 0$. Similarly, for Bob: $\bar{n}_\beta = \bar{n}_B - Y_1 - Y_2 + \frac{1}{2}$. The fractional signal mean photon numbers received by Charlie from Alice and Bob are

$$N_C^A = \eta_1 \eta_2 \bar{n}_\alpha = \eta_1 \eta_2 \left(\bar{n}_A - X_1 - X_2 + \frac{1}{2} \right) \quad (6)$$

$$N_C^B = (1 - \eta_1) \eta_2 \left(\bar{n}_B - Y_1 - Y_2 + \frac{1}{2} \right). \quad (7)$$

C. Coherent Receivers

Coherent receivers are either homodyne or heterodyne. Both designs are realizable in practice. Homodyne detection measures a single quadrature, and is described by the positive operator-valued measure (POVM) $\hat{\Pi}_q = |q\rangle\langle q|$, for $q \in \mathcal{R}$, where $|q\rangle$ are eigenstates of the real quadrature component $\hat{q} = \text{Re}(\hat{a})$ of annihilation operator \hat{a} .

If we let Alice and Bob both transmit squeezed states with means $\bar{\boldsymbol{\alpha}} = [\bar{\alpha}_1 \ \bar{\alpha}_2]^\top$ and $\bar{\boldsymbol{\beta}} = [\bar{\beta}_1 \ \bar{\beta}_2]^\top$ the quadrature mean and variance at Charlie are $\bar{x}_1 = \sqrt{\eta_1 \eta_2} \bar{\alpha}_1 + \sqrt{(1 - \eta_1) \eta_2} \bar{\beta}_1$ and $V_1 = \frac{1}{4}(\eta_1 \eta_2 e^{-2r_A} + (1 - \eta_1) \eta_2 e^{-2r_B} + (1 - \eta_2)(2\bar{n}_T + 1))$

with a similar expression for V_2 . Homodyne detection measurement outcomes are governed by the Gaussian distribution conditioned on the quadrature mean \bar{x}_1 of Charlie's state

$$p(q|\bar{x}_1) = \frac{1}{\sqrt{2\pi V_1}} \exp\left(-\frac{(q - \bar{x}_1)^2}{2V_1}\right). \quad (8)$$

Since the choice of homodyne receiver induces an additive white Gaussian noise (AWGN) channel, its capacity is maximized for a Gaussian input. The capacity of squeezed state homodyne detection for the Alice-to-Charlie channel in Fig. 1b is [34, eq. 7.51]

$$C_{\text{hom}} = \frac{1}{2} \log\left(1 + \frac{4(\bar{n}_\alpha + \frac{(1-\eta_1)\bar{n}_\beta}{\eta_1})}{e^{2r_A} + \frac{(1-\eta_1)}{\eta_1}e^{2r_B} + \frac{1-\eta_2}{\eta_1\eta_2}(1+2\bar{n}_T)}\right). \quad (9)$$

Note that setting $r_A = r_B = 0$ yields the coherent-state homodyne detection capacity.

One can describe heterodyne detection as homodyne detection along both quadratures. The heterodyne detection capacity derivation follows similarly to that of homodyne described above with a POVM $\hat{\Pi}_a = \frac{1}{\pi}|a\rangle\langle a|$ where $|a\rangle$ are eigenstates of \hat{a} . It is maximized when coherent states are employed ($r_A = r_B = 0$). The capacity of coherent-state heterodyne detection is [34, eq. 7.43]

$$C_{\text{het}} = \log\left(1 + \frac{\eta_1\bar{n}_A + (1-\eta_1)\bar{n}_B}{1 + \frac{1-\eta_2}{\eta_2}(1+2\bar{n}_T)}\right), \quad (10)$$

and for individual rate heterodyne and homodyne detection:

$$C_{\text{hetA}} = C_{\text{het}}|_{\bar{n}_B=0}, \quad C_{\text{hetB}} = C_{\text{het}}|_{\bar{n}_A=0} \quad (11)$$

$$C_{\text{homA}} = C_{\text{hom}}|_{\bar{n}_B=0}, \quad C_{\text{homB}} = C_{\text{hom}}|_{\bar{n}_A=0}. \quad (12)$$

For a full quantum description of these detection schemes, refer to [32, Section II.E] and references therein.

D. Quantum Gaussian MAC Capacity Region

Yen and Shapiro extended the Holevo-Sohma-Hirota classical capacity of quantum point-to-point Gaussian channels for squeezed states [3] to two users [13], [14]. They found that the capacity region of the quantum Gaussian channel is given by a piecewise function, which we restate here using the following three functions:

$$G_{11}(N) = g\left(V_1 + V_2 + N - \frac{1}{2}\right), \quad (13)$$

$$G_{12}(N) = g\left(2\left[-\left(\sqrt{\left(\frac{V_1 - V_2}{2}\right)^2 + V_{12}^2} - \frac{N}{2}\right)^2 + \left(\frac{V_1 + V_2 + N}{2}\right)^2\right]^{\frac{1}{2}} - \frac{1}{2}\right), \quad (14)$$

$$G_2 = g\left(2|\mathbf{V}|^{1/2} - \frac{1}{2}\right) \quad (15)$$

where $g(\cdot)$ is defined as

$$g(x) \equiv (1+x)\log(1+x) - x\log x. \quad (16)$$

The sum-rate for the MAC is

$$R_{\text{maxAB}} = \begin{cases} R_{\text{maxAB1}} & \text{if } N_C^{A+B} \geq \sqrt{(V_1 - V_2)^2 + 4V_{12}^2} \\ R_{\text{maxAB2}} & \text{if } N_C^{A+B} < \sqrt{(V_1 - V_2)^2 + 4V_{12}^2} \end{cases} \quad (17)$$

where $N_C^{A+B} = N_C^A + N_C^B$, $R_{\text{maxAB1}} = G_{11}(N_C^{A+B}) - G_2$, and $R_{\text{maxAB2}} = G_{12}(N_C^{A+B}) - G_2$. The individual rate is

$$R_{\text{maxA}} = \begin{cases} R_{\text{maxA1}} & \text{if } N_C^A \geq \sqrt{(V_1 - V_2)^2 + 4V_{12}^2} \\ R_{\text{maxA2}} & \text{if } N_C^A < \sqrt{(V_1 - V_2)^2 + 4V_{12}^2} \end{cases} \quad (18)$$

where $R_{\text{maxA1}} = G_{11}(N_C^A) - G_2$, and $R_{\text{maxA2}} = G_{12}(N_C^A) - G_2$. An expression for R_{maxB} is obtained by swapping N_C^A with N_C^B . For the states we are interested in, $V_{12} = 0$ and the threshold in (18) evaluates to $N_C^A \leq |V_1 - V_2|$. A similar condition also holds for (17).

E. Capacity-Achieving Code

Consider input with block size of M bits and codewords of length n . Then a channel code's rate is $R = M/n$ bits/symbol. Let $\hat{\rho}(\alpha)$ be a coherent state with mean $\alpha \in \mathbb{C}$. Then suppose the encoder generates 2^{nR} codewords for codebook $\mathcal{C} = \{\otimes_{m=1}^n \hat{\rho}_k(\alpha_m)\}_{k=1}^{2^{nR}}$ each according to $p(\otimes_{m=1}^n \hat{\rho}_k(\alpha_m)) = \prod_{m=1}^n p(\alpha_m)$, where $p(\alpha) = e^{-|\alpha|^2/\bar{n}}/(\pi\bar{n})$, $\otimes_{i=1}^n$ is the n -mode tensor product, and \bar{n} is the mean photon number per symbol. Yen and Shapiro showed that such a random code combined with a joint measurement receiver maximizes the sum rate R_{maxAB} for the pure-loss bosonic MAC. Moreover, such encoding also was shown to be optimal for the sum rate for the generalized phase-insensitive bosonic MAC [21]. We employ this code in the next section.

III. THERMAL-NOISE LOSSY BOSONIC MULTIPLE ACCESS CHANNEL CAPACITY

In this section we investigate the capacity for the thermal-noise lossy bosonic MAC and its asymptotic limits.

A. Fixed Mean Photon-number Constraints

For the sum-rate R_{maxAB} , substituting (4), (6), and (7) into $G_{11}(N)$ yields $G_{11}(N_C^{A+B}) = g(\bar{n}_T + (\bar{n}_B - \bar{n}_T + (\bar{n}_A - \bar{n}_B)\eta_1)\eta_2)$, without squeezing parameter dependence. Similarly, $G_{12}(N_C^{A+B})$ is strictly smaller than $G_{11}(N_C^{A+B})$. Thus maximization of R_{maxAB} reduces to the minimization of G_2 , or $|\mathbf{V}|$, as $g(\cdot)$ is monotonic. The minimum occurs for coherent-state inputs ($r_A = r_B = 0$) and matches the results in [13], [14], [21].

We next turn to the individual rates defined by R_{maxA} (and R_{maxB}). Under a global mean photon-number constraint, \bar{n}_S , for both the transmitters, let the fractional photon-number constraint for Alice be $\bar{n}_A = s\bar{n}_S$ and likewise for Bob, $\bar{n}_B = (1-s)\bar{n}_S$ where $s \in [0, 1]$. We assume Alice and

Bob can control s . Only the photons Bob uses for squeezing affect Alice's rate as they introduce additional noise in the channel. In this case, we can treat the channel as a point-to-point channel from Alice to Charlie with a mean photon-number constraint \bar{n}_S such that $s\bar{n}_S$ photons are used for the signal and $(1-s)\bar{n}_S$ photons are used for squeezing by the transmitter. It was conjectured in [5] and later proven in [6] that for the point-to-point thermal-noise lossy bosonic channel, the capacity is reached with coherent-state encoding. For a general point-to-point lossy thermal-noise channel, given \bar{x} as the mean photon-number of the signal from the transmitter at the receiver and \bar{y} as the mean photon-number of the thermal noise at the receiver, the capacity is:

$$C(\bar{x}, \bar{y}) = g(\bar{x} + \bar{y}) - g(\bar{y}). \quad (19)$$

Thus, the capacity of Alice-to-Charlie channel when Bob inputs vacuum is:

$$C_A = C(\eta_1 \eta_2 \bar{n}_A, (1 - \eta_2) \bar{n}_T). \quad (20)$$

For our two-user thermal-noise MAC, the ultimate upper bound (ub) for the individual rate ignores the interference from the other user. This corresponds to an unphysical receiver that can undo the beamsplitter between the two transmitters yielding

$$R_{\max A} \leq R_{\text{ub}A} = C(\eta_2 \bar{n}_A, (1 - \eta_2) \bar{n}_T) \quad (21)$$

$$R_{\max B} \leq R_{\text{ub}B} = C(\eta_2 \bar{n}_B, (1 - \eta_2) \bar{n}_T). \quad (22)$$

If the mean photon-number constraints are for the individual transmitters, coherent-state encoding does not necessarily maximize the individual rates for the lossy thermal-noise bosonic MAC. While squeezing does not encode information directly, an example showing that squeezed states outperform encoding using only coherent states is shown in Fig. 2. The non-linear optimization of squeezing parameters is analytically intractable. However, a numeric search quickly shows whether or not squeezing helps and the corresponding values for the squeezing parameters. In Fig. 3 we plot the capacity rate region for coherent homodyne, coherent heterodyne, coherent Gaussian encoding, an example of using squeezed states, and the individual rate outer bound in (21). In this example, utilizing squeezed states pushes out R_A beyond the coherent Gaussian encoding envelope at the expense of reduced R_B .

B. Asymptotics of Photon-Number Constraints

The sum rate capacity is achieved through the use of coherent Gaussian states, [6], [21],

$$R_A + R_B \leq C(\eta_2(\eta_1 \bar{n}_A + (1 - \eta_1) \bar{n}_B), (1 - \eta_2) \bar{n}_T), \quad (23)$$

where the RHS is equivalent to substituting coherent states in (17) and $C(\bar{x}, \bar{y})$ is defined in (19). Now, we evaluate the scaling of the individual rate for Alice with respect to the upper bounds in (21) in the case of asymptotically large input power noting that the same process applies for Bob and (22).

Lemma 1: A random code with coherent-state encoding with heterodyne detection achieves the individual rate capacity of

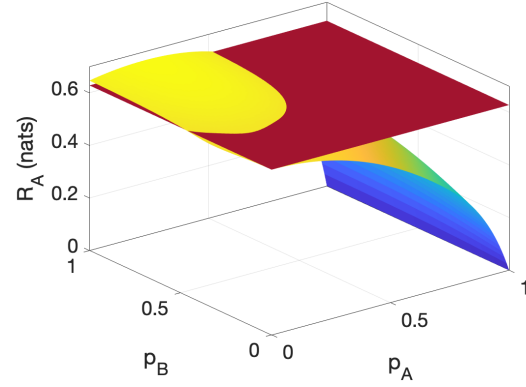


Fig. 2. Individual rates generated for all possible squeezed states given input parameters $\bar{n}_A = 4, \bar{n}_B = 8, \bar{n}_T = 4, \eta_1 = 0.2, \eta_2 = 0.9$. $p_A = \sinh^2(r_A)/\bar{n}_A$ and $p_B = \sinh^2(r_B)/\bar{n}_B$ are fractions of the total photon number utilized for squeezing by Alice and Bob respectively. The dark red plane indicates the rate achieved utilizing coherent-state encoding ($p_A = p_B = 0$) at both transmitters.

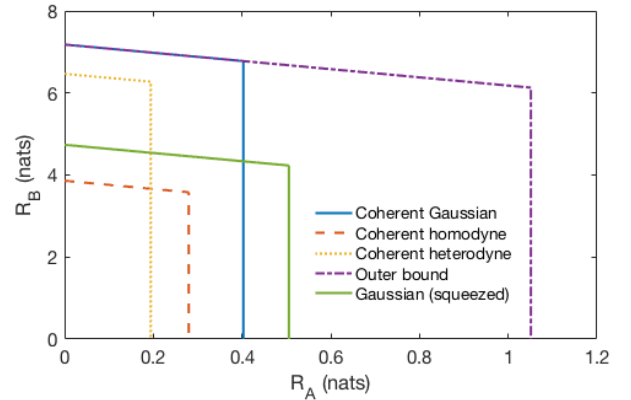


Fig. 3. Capacity region given for rates (17), (18) (and corresponding $R_{\max B}$) for the use of coherent Gaussian states and joint detection, coherent homodyne, coherent heterodyne detection, Gaussian squeezed states, and the outer bound defined in (21). Here, $\bar{n}_A = 1, \bar{n}_B = 1000, \bar{n}_T = 1, \eta_1 = 0.25, \eta_2 = 0.9$, and in the case of the squeezed state region, $r_A = 0, r_B = 3$.

the thermal-noise lossy bosonic MAC in the asymptotic limit of large transmitter input power with constant thermal noise.

Proof: For coherent-state inputs ($r_A = r_B = 0$) at Alice and Bob and a heterodyne detector at the receiver, Charlie, the capacities $C_{\text{het}A}$ and $C_{\text{het}B}$ are given by (11). Then

$$\lim_{\bar{n}_A \rightarrow \infty} \frac{C_{\text{het}A}}{R_{\text{ub}A}} = \lim_{\bar{n}_B \rightarrow \infty} \frac{C_{\text{het}B}}{R_{\text{ub}B}} = 1. \quad (24)$$

Evaluation of the limits are performed using L'Hôpital's rule and derived in Appendix A. Hence, coherent-state encoding with heterodyne detection yields the individual rate upper bounds as $\bar{n}_A \rightarrow \infty$ and $\bar{n}_B \rightarrow \infty$. ■

For homodyne detection utilizing coherent states or squeezed states, the scaling of the individual rate for Alice with respect to the upper bound in (21) is evaluated as follows:

$$\lim_{\bar{n}_A \rightarrow \infty} \max_{r_A} \lim_{\bar{n}_B \rightarrow \infty} \max_{r_B} \frac{C_{\text{hom}}}{R_{\text{ub}A}} = \frac{1}{2}, \quad (25)$$

where the maximization over r_B in the inner limit as $\bar{n}_B \rightarrow \infty$ puts all the energy available to Bob into squeezing, that is, optimal $r_B \rightarrow -\infty$. This contrasts the pure-loss channel result in [13], [14] where (25) evaluates to unity.

Lemma 2: In the limit of small photon number and constant thermal noise, utilizing a random code with coherent-state encoding at Alice and Bob and a joint detection receiver at Charlie achieves the capacity of the thermal-noise lossy bosonic MAC.

Proof: We evaluate the following three cases corresponding to the order in which photon numbers input by Alice and Bob decay to zero:

$$(i) \quad \lim_{\bar{n}_A \rightarrow 0} \lim_{\bar{n}_B \rightarrow 0} \frac{R_{\max A}}{C_A} = 1 \quad (26)$$

Bob's photon number decays to zero first. Since, effectively, he has no photons for squeezing, $N_C^A \geq |V_1 - V_2|$ and $R_{\max A} = R_{\max A1}$. Hence, the MAC reduces to a point-to-point channel in which Alice's signal photon number is attenuated by an $\eta_1 \eta_2$ term and coherent-state encoding achieves the capacity C_A in (20). This demonstrates that (21) can be made tighter in the asymptotic limit of small input power. Limits in (26) are evaluated by inspection.

$$(ii) \quad \lim_{\bar{n}_B \rightarrow 0} \lim_{\bar{n}_A \rightarrow 0} \frac{R_{\max A}}{C_A} = 1 \quad (27)$$

We allow Bob to perform an arbitrary amount of squeezing, setting his squeezing parameter to $r_B = \sinh^{-1}(\sqrt{\bar{n}_B})$. If Alice's input photon number decays to zero first, $N_C^A < |V_1 - V_2|$ and $R_{\max A} = R_{\max A2}$. The first limit ($\bar{n}_A \rightarrow 0$) is evaluated using a single application of L'Hôpital's rule, yielding a simple expression that allows the second limit ($\bar{n}_B \rightarrow 0$) to be evaluated by inspection. Details are in Appendix B1.

Finally, let $\bar{n}_A = a\bar{n}$, $\bar{n}_B = b\bar{n}$ with arbitrary constants $a, b > 0$. We show that

$$(iii) \quad \lim_{\bar{n} \rightarrow 0} \frac{R_{\max A}}{C_A} = 1. \quad (28)$$

First consider $N_C^A \geq |V_1 - V_2|$ when $R_{\max A} = R_{\max A1}$. Then any squeezing at Alice is sub-optimal because

$$G_{11}(N_C^A) = g(\eta_1 \eta_2 a \bar{n} + (1 - \eta_1) \eta_2 b \bar{n} + (1 - \eta_2) \bar{n}_T)$$

is a function of the total photon number $a\bar{n}$ at Alice and does not depend on squeezing parameter r_A . Furthermore $|V|$ in (15) is minimized for coherent-state input at Alice. Therefore, since $g(\cdot)$ is monotonic, $R_{\max A1}$ is maximized by setting $r_A = 0$. When Bob and Alice both use coherent-state encoding:

$$\lim_{\bar{n} \rightarrow 0} \frac{R_{\max A1}|_{r_A=r_B=0}}{C_A} = 1. \quad (29)$$

To show that any squeezing at Bob's transmitter cannot help, we first note that the only impact from Bob's transmissions on $R_{\max A1}$ is through transmission of squeezed states. Suppose that Bob is allowed to squeeze arbitrarily. As b is arbitrary, let Bob's squeezing parameter be $r_B = \sinh^{-1}(\sqrt{b\bar{n}})$, and Alice is transmitting an optimal coherent state ($r_A = 0$) as discussed previously. However, the constraint $N_C^A \geq |V_1 - V_2|$ upper bounds b as

$$b_{\max A1} \leq \frac{\eta_1 - 1 + \sqrt{1 + \eta_1(2 - \eta_1(1 - 4a^2\bar{n}^2))}}{2(1 - \eta_1)\bar{n}}. \quad (30)$$

Note that b is dependent on \bar{n} . Then, to upper bound Bob's possible arbitrary squeezing, let $b = \kappa b_{\max A1}$ where κ is arbitrary and $\kappa \in [0, 1]$. Hence the limit involving $R_{\max A1}$ becomes

$$\lim_{\bar{n} \rightarrow 0} \frac{R_{\max A1}|_{r_A=0, r_B=\sinh^{-1}(\sqrt{\kappa b_{\max A1} \bar{n}})}}{C_A} = 1. \quad (31)$$

Evaluation of the limit involves an application of L'Hôpital's rule and is shown in Appendix B2. Thus, squeezing does not help when $N_C^A \geq |V_1 - V_2|$.

Now consider $N_C^A < |V_1 - V_2|$ when $R_{\max A} = R_{\max A2}$. For Gaussian state inputs, $G_{12}(N_C^A) = g(2\sqrt{V_1}(\eta_1 \eta_2 p_A a \bar{n} + V_2) - \frac{1}{2})$ for $V_1 > V_2$ (with V_1 and V_2 swapped when $V_2 > V_1$), where $p_A \in [0, 1]$ is the fraction of photons Alice uses for displacement and $(1 - p_A)$ the fraction used for squeezing. Additionally, for coherent-state encoding, $G_{11}(N_C^A) = g(\eta_1 \eta_2 a \bar{n} + (1 - \eta_2) \bar{n}_T)$. Now

$$\lim_{\bar{n} \rightarrow 0} \frac{G_{12}(N_C^A)}{G_{11}(N_C^A)|_{r_A=r_B=0}} = 1, \quad (32)$$

which is derived using meticulous expansion of the terms and taking their corresponding limit in Appendix B3. Thus, because the definitions of $R_{\max A1}$ and $R_{\max A2}$ include G_2 terms

$$\lim_{\bar{n} \rightarrow 0} \frac{R_{\max A2}}{R_{\max A1}|_{r_A=r_B=0}} \leq 1. \quad (33)$$

Squeezing by Alice or Bob increases G_2 as $g(\cdot)$ is monotonic, and when $\bar{n}_T > 0$, $|V|$ is an increasing function of r_A and r_B . Thus, including G_2 terms causes the numerator of (32) to decay faster than the denominator. Therefore, any squeezing by Alice and Bob in $R_{\max A2}$ is at best equivalent to the optimal rate defined by $R_{\max A1}$ with $r_A = r_B = 0$ in the asymptotic limit of small input power.

Employing Bob's maximum rate $R_{\max B}$ and corresponding $C_A = C((1 - \eta_1) \eta_2 \bar{n}_B, (1 - \eta_2) \bar{n}_T)$ instead of $R_{\max A}$ results in limits above also evaluating to 1 as expected. ■

We note that when we replace $R_{\max A}$ in (28) with coherent or squeezed homodyne or coherent heterodyne capacities, the limit evaluates to zero. Therefore achieving bosonic MAC capacity requires more complex receiver designs.

IV. DISCUSSION

When there is a total mean photon-number constraint on the system, Alice and Bob can do no better than coherent-state encoding, allocating all of the power to Alice or Bob, depending on the transmission goal. For individual mean photon-number constraints, or when Alice and Bob do not have control over total power allocation, Figs. 2 and 3 show that squeezing can improve the individual rates when system parameters. However, in Lemmas 1-2 we prove that in asymptotic regimes of either very high or very low SNR, coherent-state encoding is optimal at the transmitters. In the case of high SNR, heterodyne detection achieves outer bound, however in the low SNR regime, neither homodyne nor heterodyne achieve the capacity.

ACKNOWLEDGMENT

The authors thank Saikat Guha for helpful and insightful discussion.

APPENDIX

The limits in Section III are derived utilizing the properties found in most undergraduate calculus textbooks. We list them here for reference. For arbitrary real-valued functions $f(x), h(x)$ and constant c :

$$\lim_{x \rightarrow a} cf(x) = c \lim_{x \rightarrow a} f(x) \quad (34)$$

$$\lim_{x \rightarrow a} f(x)h(x) = \lim_{x \rightarrow a} f(x) \lim_{x \rightarrow a} h(x) \quad (35)$$

$$\lim_{x \rightarrow a} \frac{f(x)}{h(x)} = \frac{\lim_{x \rightarrow a} f(x)}{\lim_{x \rightarrow a} h(x)}, \text{ if } \lim_{x \rightarrow a} h(x) \neq 0 \quad (36)$$

$$\lim_{x \rightarrow a} f(x) \pm h(x) = \lim_{x \rightarrow a} f(x) \pm \lim_{x \rightarrow a} h(x) \quad (37)$$

$$\lim_{x \rightarrow a} f(h(x)) = f(\lim_{x \rightarrow a} h(x)), \quad (38)$$

where the limits must exist and (38) is applicable only when $\lim_{x \rightarrow a} h(x)$ is in the domain of f . (38) allows for L'Hôpital's rule to be applied as well as two useful instances in our limits: $\lim_{x \rightarrow a} \log(f(x)) = \log(\lim_{x \rightarrow a} f(x))$ and $\lim_{x \rightarrow a} \sqrt{f(x)} = \sqrt{\lim_{x \rightarrow a} f(x)}$ when $f(a) > 0$.

We also use the following on hyperbolic trigonometric identities:

$$\cosh x = \frac{1}{2}(e^x + e^{-x}) \quad (39)$$

$$\sinh x = \frac{1}{2}(e^x - e^{-x}) \quad (40)$$

$$e^{\sinh^{-1} \sqrt{x}} = \sqrt{x} + \sqrt{x+1} \quad (41)$$

We denote the first and second derivatives of the function $f(x)$ by $f'(x)$ and $f''(x)$.

A. Evaluation of the Limit in (24) in the Proof of Lemma 1

Taking the forms of C_{hetA} and R_{ubA} in (11), (21) respectively and applying (36) to (24) yields the indeterminate form of ∞/∞ . The first application of L'Hôpital's rule with derivatives taken with respect to \bar{n}_A yields:

$$\lim_{\bar{n}_A \rightarrow \infty} \frac{C'_{\text{hetA}}}{R'_{\text{ubA}}} \quad (42)$$

$$= \lim_{\bar{n}_A \rightarrow \infty} \frac{\eta_1 \eta_2}{\eta_2 + (1 - \eta_2)(1 + 2\bar{n}_T) + \eta_1 \eta_2 \bar{n}_A} \quad (43)$$

Where $\gamma = \eta_2(\log(1 + \eta_2 \bar{n}_A + (1 - \eta_2)\bar{n}_T) - \log(\eta_2 \bar{n}_A + (1 - \eta_2)\bar{n}_T))$. Applying (36) to (43) yields the indeterminate form of 0/0 and hence a second application of L'Hôpital's rule yields a simplified form

$$\lim_{\bar{n}_A \rightarrow \infty} \frac{C''_{\text{hetA}}}{R''_{\text{ubA}}} \quad (44)$$

$$= \lim_{\bar{n}_A \rightarrow \infty} \frac{k_2}{(1 + \eta_1 \eta_2 \bar{n}_A + 2(1 - \eta_2)\bar{n}_T)^2} = 1. \quad (45)$$

Where $k_2 = \eta_1^2(\eta_2(\bar{n}_A - \bar{n}_T) + \bar{n}_T)(1 + \eta_2(\bar{n}_A - \bar{n}_T) + \bar{n}_T)$ and the limit is evaluated through the application of the properties of limits described earlier noting that the highest order terms in both the numerator and denominator are equivalent to $\eta_1^2 \eta_2^2 \bar{n}_A^2$.

B. Limit Evaluations for the Proof of Lemma 2

1) *Evaluation of the Limit in (27)* : Taking the functional forms of the numerator and denominator defined in (18) and (20), and taking their limits as $\bar{n}_A \rightarrow 0$ gives the indefinite form of 0/0, hence we can apply L'Hôpital's rule.

First note that C_A is defined in terms of $C(\bar{x}, \bar{y})$. The derivative with respect to \bar{x} of $C(\bar{x}, \bar{y})$ is

$$C'(\bar{x}, \bar{y}) = \log(1 + \bar{x} + \bar{y}) - \log(\bar{x} + \bar{y}). \quad (46)$$

Then we can define the derivative of C_A with respect to \bar{n}_A as

$$C'_A = \eta_1 \eta_2 C'(\eta_1 \eta_2 \bar{n}_A, (1 - \eta_2)\bar{n}_T), \quad (47)$$

noting the additional constant factor of $\eta_1 \eta_2$.

Next, recalling $R_{\text{maxA2}} = G_{12}(N_C^A) - G_2$, we simplify $G_{12}(N_C^A)$ when Alice is using coherent states:

$$G_{12}(N_C^A) = g \left(2\sqrt{V_1(\eta_1 \eta_2 \bar{n}_A + V_2)} - \frac{1}{2} \right). \quad (48)$$

G_2 is the same as in (15), noting no dependence on \bar{n}_A due to Alice's use of coherent states. Then R'_{maxA2} with respect to \bar{n}_A is

$$R'_{\text{maxA2}} = G'_{12}(N_C^A) + G'_2 + 0 \quad (49)$$

$$= \frac{\eta_1 \eta_2 V_1}{\sqrt{V_1(\eta_1 \eta_2 \bar{n}_A + V_2)}} \quad (50)$$

$$\times \log \left(\frac{1 + 4\sqrt{V_1(\eta_1 \eta_2 \bar{n}_A + V_2)}}{-1 + 4\sqrt{V_1(\eta_1 \eta_2 \bar{n}_A + V_2)}} \right). \quad (51)$$

Through L'Hôpital's rule

$$\lim_{\bar{n}_B \rightarrow 0} \lim_{\bar{n}_A \rightarrow 0} \frac{R'_{\text{maxA2}}}{C'_A} \quad (52)$$

$$= \lim_{\bar{n}_B \rightarrow 0} \lim_{\bar{n}_A \rightarrow 0} \frac{G'_{12}(N_C^A)}{\eta_1 \eta_2 C'(\eta_1 \eta_2 \bar{n}_A, (1 - \eta_2)\bar{n}_T)} \quad (53)$$

$$= \lim_{\bar{n}_B \rightarrow 0} \frac{\frac{V_1}{\sqrt{V_1 V_2}} \log \left(\frac{1 + 4\sqrt{V_1 V_2}}{-1 + 4\sqrt{V_1 V_2}} \right)}{\log(1 + \frac{1}{(1 - \eta_2)\bar{n}_T})}, \quad (54)$$

where the limit of \bar{n}_A can be evaluated by inspection and utilizing the properties of limits defined previously. In order to perform the limit of $\bar{n}_B \rightarrow 0$, we first expand V_1 and V_2 :

$$V_1 = \frac{1}{4}(1 - \eta_2)(2\bar{n}_T + 1) + \frac{1}{4}(1 - \eta_1)\eta_2 e^{\sinh^{-1}(\sqrt{\bar{n}_B})} + \frac{1}{4}\eta_1 \eta_2 \quad (55)$$

$$V_2 = \frac{1}{4}(1 - \eta_2)(2\bar{n}_T + 1) + \frac{1}{4}(1 - \eta_1)\eta_2 e^{-\sinh^{-1}(\sqrt{\bar{n}_B})} + \frac{1}{4}\eta_1 \eta_2. \quad (56)$$

Using (38) and (35) we only need to perform the limit for V_1 and V_2 : $\lim_{\bar{n}_B \rightarrow 0} V_1 = \lim_{\bar{n}_B \rightarrow 0} V_2 = \frac{1}{4}((1 - \eta_2)(2\bar{n}_T + 1) + \eta_1 \eta_2)$, and hence (54) evaluates to unity.

2) *Evaluation of the Limit in (31)*: Applying the properties of limits to the limit in (31) yields an indeterminate form of 0/0 and we rely on L'Hôpital's rule. The derivative with respect to \bar{n} in the denominator, C'_A , has no b dependence and is given by:

$$C'_A = a\eta_1\eta_2[\log(1 + \eta_1\eta_2a\bar{n}(1 - \eta_2)\bar{n}_T) - \log(\eta_1\eta_2a\bar{n} + (1 - \eta_2)\bar{n}_T)]. \quad (57)$$

This limit can be performed by inspection,

$$\lim_{\bar{n} \rightarrow 0} C'_A = a\eta_1\eta_2[\log(1 + (1 - \eta_2)\bar{n}_T) - \log((1 - \eta_2)\bar{n}_T)]. \quad (58)$$

The derivative of the numerator, $R'_{\max A1}|_{r_A=0, r_B=\sinh^{-1}(\sqrt{\kappa b_{\max A1}\bar{n}})}$, can be split into two parts as $R'_{\max A1} = G'_{11}(N_C^A) - G'_2$. Taking the derivative of the two terms yields

$$G'_{11}(N_C^A) = \frac{\theta_2}{\theta_1}(\log(1 + \theta_3) - \log(\theta_3)) \quad (59)$$

$$G'_2 = \frac{\theta_5}{\theta_1\theta_4}(\log(1 + \theta_4) - \log(-1 + \theta_4)), \quad (60)$$

where

$$\theta_1 = [1 - \eta_1(2 - \eta_1 - 4a^2\eta_1\bar{n}^2)]^{\frac{1}{2}} \quad (61)$$

$$\theta_2 = a\eta_1\eta_2(2a\eta_1\kappa\bar{n} + \theta_1) \quad (62)$$

$$\theta_3 = a\eta_1\eta_2\bar{n} - \frac{1}{2}\eta_2\kappa(1 - \eta_1 - \theta_1) + (1 - \eta_1)\bar{n}_T \quad (63)$$

$$\theta_4 = [2\eta_2\kappa(\eta_1 + \theta_1 - 1)(1 - \eta_2(1 - \eta_1 + 2\bar{n}_T) + \bar{n}_T) + (1 + 2(1 - \eta_2)\bar{n}_T)^2]^{\frac{1}{2}} \quad (65)$$

$$\theta_5 = 2a^2\eta_1^2\eta_2\kappa\bar{n}(1 - \eta_2(1 - \eta_1 + 2\bar{n}_T) + 2\bar{n}_T). \quad (66)$$

Using (37) we can additionally split the limit into two parts. In order to take the limit as $\bar{n} \rightarrow 0$ of (60), note that the denominator and log terms are strictly non-zero as θ_4 and θ_1 only have partial \bar{n} dependence, additionally θ_5 has an \bar{n} factor which goes to 0, hence

$$\lim_{\bar{n} \rightarrow 0} G'_2 = 0. \quad (67)$$

To find the limit as $\bar{n} \rightarrow 0$ of (59) we apply (36) and take the limits of the numerator and denominator. While the equations are lengthy, the limits can be performed through inspection and use of eqs. (34)-(38). After the limit is evaluated through inspection additional algebraic steps can be performed to simplify as

$$\lim_{\bar{n} \rightarrow 0} G'_{11} = a\eta_1\eta_2[\log(1 + (1 - \eta_2)\bar{n}_T) - \log((1 - \eta_2)\bar{n}_T)]. \quad (68)$$

This matches the results of the limit in (58) and hence the limit in (31) evaluates to unity.

3) *Evaluation of the Limit in (32)*: For an arbitrary amount of squeezing at Bob, as in the previous limits, $r_B = \sinh^{-1}(\sqrt{b\bar{n}})$. We define p_A to be the fraction of photons Alice uses for her signal and $(1 - p_A)$ are used for squeezing. Therefore $r_A = \sinh^{-1}(\sqrt{a(1 - p_A)\bar{n}})$. Here,

$$V_1 = \frac{1}{4}((1 - \eta_2)(2\bar{n}_T + 1) + (1 - \eta_1)\eta_2e^{\sinh^{-1}(\sqrt{b\bar{n}})} + \eta_1\eta_2e^{\sinh^{-1}(\sqrt{a(1 - p_A)\bar{n}})}) \quad (69)$$

$$V_2 = \frac{1}{4}((1 - \eta_2)(2\bar{n}_T + 1) + (1 - \eta_1)\eta_2e^{-\sinh^{-1}(\sqrt{b\bar{n}})} + \eta_1\eta_2e^{\sinh^{-1}(-\sqrt{a(1 - p_A)\bar{n}})}). \quad (70)$$

Note that similar to Appendix A, $G_{12}(N_C^A) = g(2\sqrt{V_1(\eta_1\eta_2p_Aa\bar{n} + V_2)} - \frac{1}{2})$.

Additionally,

$$G_{11}(N_C^A)|_{r_A=r_B=0} = g(\eta_1\eta_2a\bar{n} + (1 - \eta_2)\bar{n}_T). \quad (71)$$

The limit can be evaluated using (36). Note that the limit for $G_{12}(N_C^A)$ only needs to be evaluated for (69) and (70) due to (38). By inspection and appropriate substitutions,

$$\lim_{\bar{n} \rightarrow 0} \frac{G_{12}(N_C^A)}{G_{11}(N_C^A)|_{r_A=r_B=0}} \quad (72)$$

$$= \frac{\lim_{\bar{n} \rightarrow 0} g(2\sqrt{V_1(\eta_1\eta_2p_Aa\bar{n} + V_2)} - \frac{1}{2})}{\lim_{\bar{n} \rightarrow 0} g(\eta_1\eta_2a\bar{n} + (1 - \eta_2)\bar{n}_T)} = 1. \quad (73)$$

REFERENCES

- [1] M. A. Nielsen and I. L. Chuang, *Quantum Computation and Quantum Information*. New York, NY, USA: Cambridge University Press, 2000.
- [2] M. Wilde, *Quantum Information Theory*, 2nd ed. Cambridge University Press, 2016.
- [3] A. S. Holevo, M. Sohma, and O. Hirota, "Capacity of quantum Gaussian channels," *Phys. Rev. A*, vol. 59, no. 3, pp. 1820–1828, Mar. 1999. [Online]. Available: <https://link.aps.org/doi/10.1103/PhysRevA.59.1820>
- [4] V. Giovannetti, S. Lloyd, L. Maccone, and P. W. Shor, "Broadband channel capacities," *Phys. Rev. A*, vol. 68, p. 062323, Dec. 2003.
- [5] V. Giovannetti, S. Guha, S. Lloyd, L. Maccone, and J. H. Shapiro, "Minimum output entropy of bosonic channels: a conjecture," *Phys. Rev. A*, vol. 70, no. 3, p. 032315, Sep. 2004.
- [6] V. Giovannetti, R. Garcia-Patron, N. J. Cerf, and A. S. Holevo, "Ultimate communication capacity of quantum optical channels by solving the Gaussian minimum-entropy conjecture," *Nature Photon*, vol. 8, no. 10, pp. 796–800, Oct. 2014.
- [7] V. Scarani, H. Bechmann-Pasquinucci, N. J. Cerf, M. Dušek, N. Lütkenhaus, and M. Peev, "The security of practical quantum key distribution," *Rev. Mod. Phys.*, vol. 81, pp. 1301–1350, Sep. 2009.
- [8] S. Pirandola, U. L. Andersen, L. Banchi, M. Berta, D. Bunandar, R. Colbeck, D. Englund, T. Gehring, C. Lupo, C. Ottaviani, J. L. Pereira, M. Razavi, J. S. Shaari, M. Tomamichel, V. C. Usenko, G. Vallone, P. Villoresi, and P. Wallden, "Advances in quantum cryptography," *Adv. Opt. Photon.*, vol. 12, no. 4, pp. 1012–1236, Dec 2020.
- [9] B. A. Bash, A. H. Gheorghie, M. Patel, J. L. Habif, D. Goeckel, D. Towsley, and S. Guha, "Quantum-secure covert communication on bosonic channels," *Nat. Commun.*, vol. 6, Oct. 2015.
- [10] M. S. Bullock, C. N. Gagatsos, S. Guha, and B. A. Bash, "Fundamental limits of quantum-secure covert communication over bosonic channels," *IEEE J. Sel. Areas Commun.*, vol. 38, no. 3, pp. 471–482, Mar. 2020.
- [11] C. N. Gagatsos, M. S. Bullock, and B. A. Bash, "Covert capacity of bosonic channels," *IEEE J. Sel. Areas Inf. Theory*, vol. 1, pp. 555–567, 2020.
- [12] A. E. Gamal and Y.-H. Kim, *Network Information Theory*. New York, NY, USA: Cambridge University Press, 2012.

- [13] B. J. Yen and J. H. Shapiro, “Multiple-access bosonic communications,” *Phys. Rev. A*, vol. 72, no. 6, p. 062312, Dec. 2005, publisher: American Physical Society. [Online]. Available: <https://link.aps.org/doi/10.1103/PhysRevA.72.062312>
- [14] B. J. Yen, “Multiple-user quantum optical communication,” Ph.D. dissertation, Massachusetts Institute of Technology, 2005.
- [15] A. Winter, “The capacity of the quantum multiple-access channel,” *IEEE Trans. Inf. Theory*, vol. 47, no. 7, pp. 3059–3065, 2001.
- [16] J. Yard, I. Devetak, and P. Hayden, “Capacity theorems for quantum multiple access channels,” in *Proc. IEEE Int. Symp. Inf. Theory (ISIT)*, 2005, pp. 884–888.
- [17] R. Ahlswede and N. Cai, *A Strong Converse Theorem for Quantum Multiple Access Channels*. Berlin, Heidelberg: Springer-Verlag, 2006, pp. 460—485.
- [18] H. Qi, Q. Wang, and M. M. Wilde, “Applications of position-based coding to classical communication over quantum channels,” *J. Phys. A: Math. Theor.*, vol. 51, no. 44, p. 444002, Oct. 2018.
- [19] M. Hayashi and N. Cai, “Universal classical-quantum multiple access channel coding,” in *Proc. IEEE Int. Symp. Inf. Theory (ISIT)*, 2021, pp. 402–407.
- [20] M. Hayashi and A. Vázquez-Castro, “Computation-aided classical-quantum multiple access to boost network communication speeds,” *Phys. Rev. Applied*, vol. 16, p. 054021, Nov 2021.
- [21] H. Shi and Q. Zhuang, “Computable limits of optical multiple-access communications,” *Phys. Rev. A*, vol. 105, p. 022429, Feb 2022. [Online]. Available: <https://link.aps.org/doi/10.1103/PhysRevA.105.022429>
- [22] H. Shi, M.-H. Hsieh, S. Guha, Z. Zhang, and Q. Zhuang, “Entanglement-assisted capacity regions and protocol designs for quantum multiple-access channels,” *npj Quantum Information*, vol. 7, no. 1, pp. 1–9, 2021.
- [23] R. Laurenza and S. Pirandola, “General bounds for sender-receiver capacities in multipoint quantum communications,” *Physical Review A*, vol. 96, no. 3, p. 032318, 2017.
- [24] A. Anshu, R. Jain, and N. A. Warsi, “On the near-optimality of one-shot classical communication over quantum channels,” *Journal of Mathematical Physics*, vol. 60, no. 1, p. 012204, 2019.
- [25] H. Aghaee and B. Akhbari, “Private classical information over a quantum multiple access channel: One-shot secrecy rate region,” in *2020 10th International Symposium on Telecommunications (IST)*. IEEE, 2020, pp. 222–226.
- [26] —, “Classical-quantum multiple access wiretap channel,” in *2019 16th International ISC (Iranian Society of Cryptology) Conference on Information Security and Cryptology (ISCISC)*. IEEE, 2019, pp. 99–103.
- [27] A. K. Sinclair, E. Schroeder, D. Zhu, M. Colangelo, J. Glasby, P. D. Mauskopf, H. Mani, and K. K. Berggren, “Demonstration of microwave multiplexed readout of DC-biased superconducting nanowire detectors,” *IEEE Trans. Appl. Supercond.*, vol. 29, no. 5, Aug. 2019.
- [28] A. N. McCaughan, D. M. Oh, and S. W. Nam, “A stochastic SPICE model for superconducting nanowire single photon detectors and other nanowire devices,” *IEEE Trans. Appl. Supercond.*, vol. 29, no. 5, Aug 2019.
- [29] J. Lee, L. Shen, A. Cerè, T. Gerrits, A. E. Lita, S. W. Nam, and C. Kurtsiefer, “Multi-pulse fitting of transition edge sensor signals from a near-infrared continuous-wave source,” *Rev. Sci. Instrum.*, vol. 89, no. 12, p. 123108, 2018.
- [30] A. S. Holevo and R. F. Werner, “Evaluating capacities of bosonic gaussian channels,” *Phys. Rev. A*, vol. 63, p. 032312, Feb 2001.
- [31] C. Lupo, S. Pirandola, P. Aniello, and S. Mancini, “On the classical capacity of quantum gaussian channels,” *Physica Scripta*, vol. T143, p. 014016, feb 2011.
- [32] C. Weedbrook, S. Pirandola, R. García-Patrón, N. J. Cerf, T. C. Ralph, J. H. Shapiro, and S. Lloyd, “Gaussian quantum information,” *Rev. Mod. Phys.*, vol. 84, pp. 621–669, May 2012.
- [33] M. Reck, A. Zeilinger, H. J. Bernstein, and P. Bertani, “Experimental realization of any discrete unitary operator,” *Phys. Rev. Lett.*, vol. 73, pp. 58–61, Jul. 1994.
- [34] S. Guha, “Classical capacity of the free-space quantum-optical channel,” Master’s thesis, Massachusetts Institute of Technology, 2004.